Modeling magnetic polarity distributions of solar activity from its helioseismic signature

A.-C. Donea[1] and C. Lindsey[2]

[1] School of Mathematics, Monash University, 9 Rainforest Walk, Clayton, VIC 3800, Australia

[2] NorthWest Research Associates, Colorado Offices, 3380 Mitchell Lane, Boulder, Colorado 30801, USA

E-mail: alina.donea@monash.edu

June 2018

Abstract. We propose to develop, as an inverse problem, the facility to assign appropriate polarities to magnetic flux distributions whose absolute magnetic field strengths, $|\mathbf{B}|^2$, are well mapped but whose local polarities (north/south) are unknown. Standard diagnostics in helioseismology, such as *computational helioseismic holography*, give us good maps of $|\mathbf{B}|^2$, of active regions in the Sun's far hemisphere, but are clueless as to where the local magnetic polarity is north or south. As a basis for assigning appropriate polarities to the elements of helioseismic signatures, we turn to the *Hale Polarity Law*, following leads introduced by N. Arge and C. Henney. The magnetic flux densities of newly emerging magnetic flux ropes are strongly bipolar. The Hale Law observes that when these fluxes are large, the leading (westward) component of the magnetic signature is consistently of south-magnetic polarity in the Sun's northern hemisphere and of north-magnetic polarity in the Sun's southern hemisphere—*currently*. This pattern reverses in both hemispheres every eleven years after a brief period—a year or two—of virtual magnetic hibernation. The next reversal is due in the early 2020s. The Hale Law renders the solution straight-forward when the emerging flux is a single, well-defined flux rope, as it often is in fact. The challenge looms when the emerging flux is more complex, resulting in multiple photospheric bipoles, sometimes with the trailing pole of one component compacted against the leading pole of some other, for example. This is important for practical applications in space-weather forecasting, because opposing magnetic poles of this vintage often interact violently, giving rise to flares and coronal mass ejections, impacting space weather at Earth—when these regions rotate into the Sun's near hemisphere.

Keywords: Sun, magnetic fields, solar activity, space weather

Submitted to: *Inverse Problems*

1. Introduction

Approaching the turn of the century, C. Lindsey and D. C. Braun [1, 2] developed algorithms in local helioseismology to compute acoustic images of active regions from helioseismic observations from the near hemisphere (see also A.-C. Donea [3]). These algorithms allowed us to acoustically *see through the solar interior* to large active regions in the Sun's far hemisphere [4]. Further developed and refined by Braun and Lindsey [5] and applied to helioseismic observations from the Helioseismic-Magnetic Imager (HMI) aboard the Solar Dynamics Observatory (SDO) and from the Global Oscillations Network Group (GONG), these facilities now provide us with daily synoptic maps of large active regions fully covering the Sun's far hemisphere (`http://jsoc.stanford.edu/data/farside`). These helioseismic maps are very useful for space-weather forecasting on time scales ranging from about a day to two weeks.‡

For most of the past decade, the needs of space-weather forecasters for monitoring the Sun's far hemisphere have been serviced by EUV observations from NASA's twin STEREO spacecraft, which have enjoyed a composite vantage that fully covers the Sun's far hemisphere. The helioseismic maps are not nearly as sensitive a monitor of solar activity as direct observations of the Sun in electromagnetic radiation. They are, nevertheless, sensitive enough to detect and accurately locate about the 400 strongest active regions in a weak solar cycle, such as the current cycle 24, i.e., essentially all of those that pose a major space weather concern at Earth. More importantly, both of NASA's STEREO spacecraft are inexorably drifting back to Earthside of the solar system, and, in 2019, will begin to lose their far-side vantage. Over the succeeding decade, there will be long periods during which electromagnetic coverage of the Sun's far hemisphere will be next to nil—during which the helioseismic monitor will maintain full coverage of the far hemisphere. Helioseismology stands, thus, at the brink of a unique and distinctive role in our world's space-weather forecasting industry into the indefinite future.

The ability of the far-side seismic monitor to detect and accurately locate active regions in the far hemisphere that pose a major concern to space-weather in the near-Earth environment is well established. Figures 1 and 2 show a sample of its forecasting capacity applied to large active regions that emerged into the Sun's southern hemishere in early November of 2014. The far-side (amber) component of the solar map shows the signatures of regions designated FS-101 and FS-103 by the SDO far-side seismic monitor, on 2014-11-05. Figure 2 shows observations of these regions 12 days thence in familiar electromagnetic radiation when they are in direct view from Earth.

Copious magnetic flux distributed over large areas, once it has broken the Sun's

‡ In point of fact, it is rare for even the strongest, most active magnetic regions to significantly impact the Earth environment from the Sun's far hemisphere. By far, the most general space-weather concern is what a strong active region will do once solar rotation brings it into the near hemisphere, in direct view from Earth. This will invariably transpire within two weeks, the nominal transit time of an active region across a solar hemipshere.

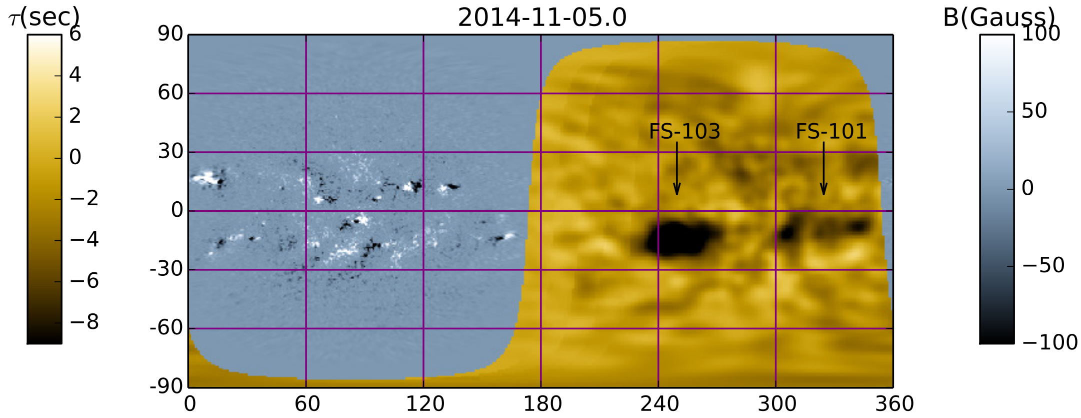

Figure 1. Composite map of the Sun on 2014-11-05.0 posted by the SDOs Joint Science Operations center (JSOC) at Stanford (see `http://jsoc.stanford.edu/data/farside`). The amber region represents the far hemisphere, showing the seismic signatures of active regions designated "FS-103" and "FS-101". The blue-gray region shows the concurrent line-of-sight magnetogram of the near hemisphere.

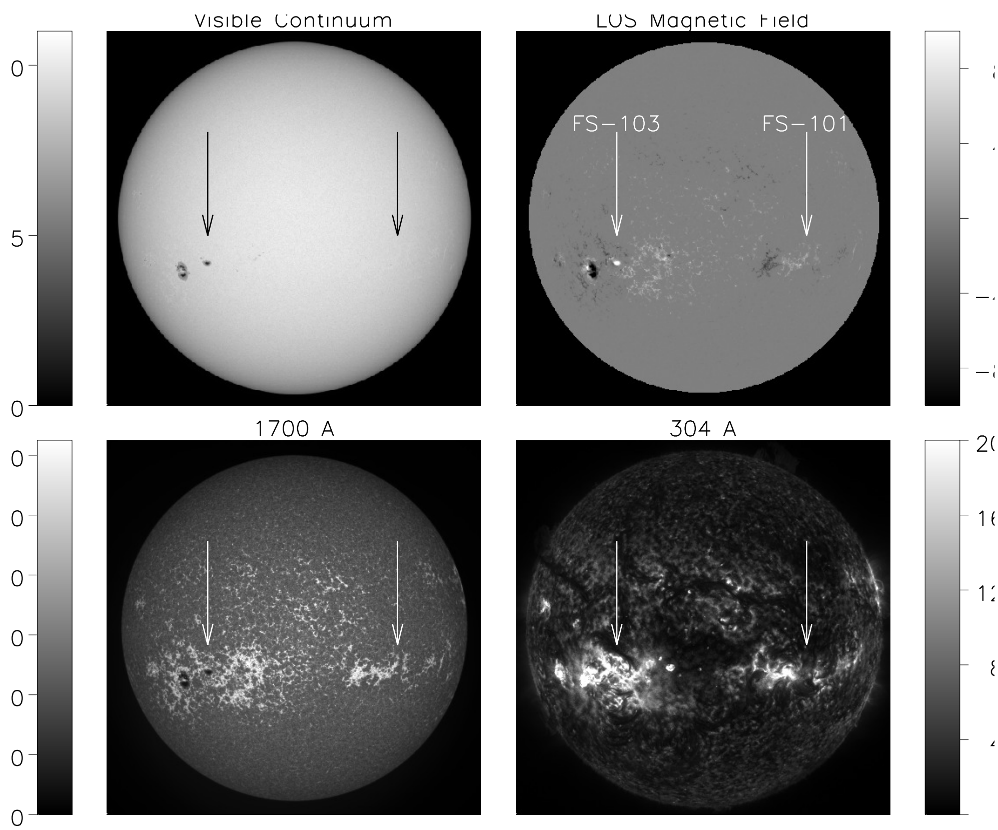

Figure 2. The Sun in visible, UV and EUV radiation on 2014-11-17, activer regions designated FS-101 and FS-103 in Figure 1 now both having rotated into direct view from Earth. Top-left: visible continuum intensity at 6370 Å; top-right: line-of-sight magnetogram from Fe I 6370 Å; bottom-left: near UV (1,700 Å) continuum intensity; bottom-right: EUV (He II 304 Å) intensity.

surface, is generally there to stay [6] until it is dissipated by diffusion (or possibly ejected or resubmerged) over months or years. In general, then, signatures in seismic maps of large active regions in the far hemisphere are a reliable predictor of excess UV and EUV irradiance at Earth during a subsequent transit across the Sun's near hemisphere of the regions indicated.

There remain major outstanding potentialities of far-side solar seismology that have yet to be fully developed. Space-weather forecasting based on observations of the Sun's *near* hemisphere, for example, enjoys detailed maps clearly showing both the signs and magnitudes of the magnetic flux densities, B_z, of active regions that impact space weather. While highly sensitive to photospheric magnitude of B_z, helioseismic signatures are invariant under reversal of its sign, hence unable to determine these, on their own. Helioseismic signatures are therefore missing much desired information on an aspect of solar activity that is crucial to space weather and its forecasting.

2. The Hale Polarity Law as a magnetic-polarity resource

Arge et al. [7] introduced the use of the Hale Polarity Law as a resource for modeling the signs (north/south) to be associated with various components of their diagnostic signatures, applied first to STEREO EUV observations of the Sun from the far side of the solar system, and then to helioseismic maps of the same. They used the results as input for their Air Force Data Assimilative Photospheric Flux Transport (ADAPT) algorithm for modeling of the Sun's global coronal magnetic field. Observations of the Sun's near hemisphere show the Hale Law to be highly reliable for large active regions, those of real concern for space-weather forecasting. This can be useful not only for assigning a flare potentiality to active regions born in the Sun's far hemisphere, but also for realistically modeling the global coronal magnetic field over the entirety of the Sun's surface. The latter utility can help us to anticipate the formation of coronal holes, which are a source of high-speed streams, causing geomagnetic storms soon after they rotate into the near hemisphere and cross central solar meridian.

González et al. [8] compiled statistics on the relationship between the strengths of helioseismic signatures of active regions in the Sun's far hemisphere and both their areas and magnetic fluxes when they subsequently appeared in the near hemisphere. These statistics suffer considerably from the evolution a magnetic region invariably undergoes between when its seismic signature is recorded in the far hemisphere and its magnetic signatures become directly visible from Earth vantage days later in the near hemisphere. In fact, active regions in the Sun's *near* hemisphere have well known helioseismic signatures there as well. MacDonald et al. [9] seized upon this resource to compile valuable statistics on the relationship between seismic and magnetic properties. This lends us a tremendous advantage, because not only are the properties so related now *concurrently observed*, the helioseismic signatures are of *much higher quality*, both in spatial resolution and signal to noise, than helioseismic signatures in the far hemisphere. Figure 3 illustrates this advantage by the example of NOAA AR11416 on 2011-12-

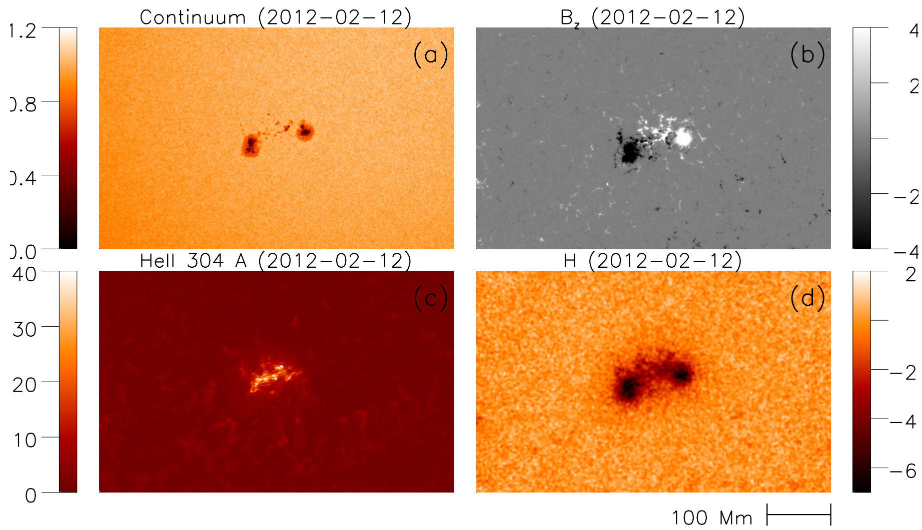

Figure 3. Seismic map of NOAA AR11416 in the Sun's near hemisphere (Frame d) is shown on 2011-02-12 concurrently and cospatially with a visible-continuum-intensity map (Frame a), a line-of-sight magnetic map (Frame b), and a He II 304 Å intensity map (Frame c).

12 as it approaches central meridian in the Sun's near hemisphere. The helioseismic signature (lower-right) is shown concurrently with visible continuum intensity (upper-left), line-of-sight magnetic field (upper-right) and EUV intensity (lower-left) in the near hemisphere.§ Among the attributes of the helioseismic signature highlighted by this example is the strong similarity in the *morphology* of the helioseismic signature to that of the magnetic flux distribution as approximated by the line-of-sight magnetic signature. This is the basis of a simple working model by Lindsey, Cally and Rempel [10] that relates helioseismic signatures of magnetic regions to an *effective magnetic depression* of the photosphere in response to the photospheric magnetic pressure,

$$p_m \equiv \frac{B^2}{8\pi}. \tag{1}$$

By comparison, the most conspicuous EUV emission tends to emanate more from footpoints of overlying coronal loops, perhaps from the loops themselves, and from strong magnetic neutral lines in the photosphere. The helioseismic signature (lower-right panel of Figure 3), then, enjoys a simpler and more direct relationship to the magnetic flux density than, for instance, the EUV source density (lower-left panel).

This study is a natural extention of the work begun by MacDonald et al. [9] and their predecessors. We want to further develop the use of the Hale Polarity Law to devise

§ At this juncture, we confront the prospect of confusion in a long tradition that applies the term "north," for example, both to local magnetic polarities in an active region and to the local projection of the Sun's rotational axis onto its surface. To avoid this, we apply "north" and "south" only in the magnetic context, refering to rotational-north simply as "upward," -south as "downward," -east as "leftward," and -west as "rightward".

realistic projections of signed magnetic flux distributions from helioseismic signatures. The basic, ground-floor approach will be to use the helioseismic signature as a proxy for the *positive magnitude of the magnetic flux density.* To do this we propose to apply an algorithmic interpretation of the Hale Polarity Law devised to assign appropriate north- and south-magnetic designations to respective components of the flux distribution so recognized.

Arge et al. [7] have already modeled the active regions whose seismic signatures they studied as simple single magnetic bipoles. The purpose of this study is to explore an extension of their algorithm to one that appropriately accommodates more complex magnetic configurations, ones that involve multiple bipoles, or perhaps continuous distributions of bipolarity. This study will be conducted in the near hemisphere on active regions therein, taking full advantage of helioseismic signatures that are of much higher quality than those of active regions in the far hemisphere. This is intended to give us understanding beyond what we can derive from similar studies comparing helioseismic signature in the far hemisphere with subsequent magnetic signatures in the near hemisphere. The intention is that this understanding will guide us in subsequent efforts to develop an algorithm to characterize signed magnetic-polarity distributions of magnetic regions in the *far* hemisphere even if this application of the algorithm cannot accomplish the spatial discrimination of its counterpart in the near hemisphere.

3. Conceptual formulation

Individual emerging magnetic fluxtubes tend to initially manifest themselves at the Sun's surface in the form of a bipole, in accordance with the Hale Law, one polarity in a given hemisphere consistently leading the other in longitude. Soon after emergence, these appear as opposing magnetic poles, and tend to drift in opposing directions while diffusing outward. This outward diffusion is not generally isotropic, but is statistically well measured [6], the mean profile of it depending significantly upon the latitude at which the flux has emerged. At the same time as the flux diffuses, it gradually precipitates into myriad compact condensations, the strongest of which become sunspots, while most settle into the intersupergranular network.

When trying to understand simple cases, such as AR11416, one wonders whether understanding the *connectivity* between north- and south-pole components of an active region can be of help in determining how to most prospectively attach north- and south-magnetic designations to distinctive components of the helioseismic signature. If so, the inclusion of connectivity in the model could bring major space-weather forecasting assets of its own. In any case, we propose to take on the problem not only of assigning magnetic northness and southness to the various regional components of helioseismic signatures, but, given a distinctive regional component that is determined to be of north polarity, a proposed location of its "magnetic conjugate region", i.e., the region at which magnetic streamlines passing through it return to the photosphere as south polarity. We will call this the pole-pairing problem.

4. The pole-pairing problem

4.1. Conceptual summary of the problem

Let $\mathcal{H}$ represent the helioseismic signature of an active region, $\mathcal{A}$, which we will express as a field $H(\boldsymbol{\rho})$ over $\mathcal{A}$, i.e.,

$$\mathcal{H}: \quad H(\boldsymbol{\rho}) \; \forall \; \boldsymbol{\rho} \; \in \; \mathcal{A}, \tag{2}$$

wherein we assume that $H(\boldsymbol{\rho})$ is null outside of $\mathcal{A}$. We define the basic pole-pairing problem as follows:

(i) How do we devise an appropriate partition, $(\mathcal{N},\ \mathcal{S})$ of $\mathcal{A}$ into two separate components, one, $\mathcal{N}$, identified with north-magnetic and the other, $\mathcal{S}$, with south-magnetic polarities of the local magnetic flux penetrating it, in a way that is most consistent with the Hale Law by some criterion? For general convenience, we include as consistency with the Hale Law the requirement the total north- and south-magnetic fluxes are equal, as required by magnetic-flux conservation.

(ii) For any given partition, $(\mathcal{N},\ \mathcal{S})$ of $\mathcal{A}$ we can devise any number of mappings,

$$\boldsymbol{\rho}_s \; \equiv \; \mathcal{W}(\boldsymbol{\rho}_n), \tag{3}$$

associating with each point, $\boldsymbol{\rho}_n$, in $\mathcal{N}$, its magnetic conjugate, $\boldsymbol{\rho}_s$, in $\mathcal{S}$.‖ The pole-pairing problem asks which of all possible of these mapping is the best one by some criterion. The mapping prescribed by $\mathcal{W}$ can be regarded as a kind of relative *warpage*, within specifications of the Hale Law, of the field $\mathcal{S}$ to conform the morphology of its helioseismic signature to that of $\mathcal{N}$. We will call $\mathcal{W}$, together with its domain, $\mathcal{N}$, a "Hale mapping", and $\mathcal{W}(\mathcal{N})$ the "Hale image" of $\mathcal{N}$ in $\mathcal{A}$, or possibly just "the image" thereof when Hale mapping is the clear context. Any given $\mathcal{N}$ can have an infinite number of different Hale mappings, $\mathcal{W}$, to which it is attached. However, any $\mathcal{W}$ is uniquely attached to a single $\mathcal{N}$, and so, no two $\mathcal{W}$-like specifications, $\mathcal{W}_1$ and $\mathcal{W}_2$, that apply to different, non-identical domains, $\mathcal{N}_1$ and $\mathcal{N}_2$, are to be regarded as equal to each other even if $\mathcal{W}_2$ is identical to $\mathcal{W}_2$ is in the intersection of $\mathcal{N}_1$ and $\mathcal{N}_2$.

With the foregoing considerations in mind, we now propose to express $\mathcal{W}$ by recognizing the displacement

$$\boldsymbol{\zeta} \; \equiv \; \boldsymbol{\rho}_s \; - \; \boldsymbol{\rho}_n \; \forall \; \boldsymbol{\rho}_n \; \in \; \mathcal{N}, \tag{4}$$

between the south-magnetic (following) pole magnetically connected to the north-magnetic (leading) pole at $\boldsymbol{\rho}_n$ in $\mathcal{N}$, and defining a function, W, that prescribes this displacement for each $\boldsymbol{\rho}$ in its domain, $\mathcal{N}$:

$$\boldsymbol{\zeta} \; = \; W(\boldsymbol{\rho}) \; \forall \; \boldsymbol{\rho} \; \in \; \mathcal{N}. \tag{5}$$

‖ In standard algebraic terminology [11], $\mathcal{W}$ is the subset of *pairs of points*, $(\boldsymbol{\rho}_n,\ \boldsymbol{\rho}_s)$ in $\mathcal{N} \times \mathcal{S}$ such that each $\boldsymbol{\rho}_s$ in $\mathcal{S}$ is proposed to be connected to its counterpart, $\boldsymbol{\rho}_n$, in $\mathcal{N}$, by a magnetic streamline.

Our understanding of actual magnetic fields implies that $\mathcal{W}$ is technically a one-to-one mapping. However, realistic helioseismic signatures frequently confront us with regions wherewithin, because of limited spatial discrimination, the helioseismic signature in any a single resolution element is a result of flux of both north- and south-magnetic flux penetrating said region. It is therefore useful to devise a scheme that can accommodate some degree of overlap between $\mathcal{N}$ and $\mathcal{S}$. This opens the discussion to consideration of Hale mappings that can be not strictly one-to-one everywhere.

We now turn to the question of how a judgement is to be made as to what Hale mapping, $\mathcal{W}$, is best for a given helioseismic signature $\mathcal{H}$.

4.2. Quality assessment of a Hale mapping

Comparisons between various possible Hale mappings and magnetic signatures of active regions in the Sun's near hemisphere make it quite evident that some Hale mappings are "better" than others, i.e., more like the actual polarities of the magnetic flux that gives rise to the helioseismic signature by some comparative criteria. There is at most only a single model that can be absolutely correct, and so, until we reach a degree of insight we have yet to approach, we confront the need to reserve a distinction between any *model* and the single (we think) *reality*. This opens the need for an ability to assign a quality, Q, to an individual $\mathcal{W}(\mathcal{H})$, hence to various schemes proposing high-quality Hale mappings. How well we can do this depends heavily upon how much we know from observations. This changes radically from before we have magnetic observations to after. In principle, both $\mathcal{N}$ and $\mathcal{W}$ can be determined in detail from vector-magnetic observations, and we might propose to call a comparison between the connectivity specifed by $\mathcal{W}$ and that determined by concurrent magnetic observations an "after-the-fact quality assessment". For a magnetic configuration whose signed polarities have yet to be observed, what we have for guidance in devising a realistic model is considerably less—but, nevertheless, considerable. Such a quality can be defined for a given helioseismic signature, $\mathcal{H}$, and Hale mapping, $\mathcal{W}$, in any of a broad variety of ways. For the exercise we will run presently, we define it in terms of a functional, $Q(\mathcal{W},\ \mathcal{H})$, operating on $(\mathcal{W},\ \mathcal{H})$ that expresses the *rms deviation*,

$$Q(\mathcal{W},\ \mathcal{H}) \ = \ \Big(\int_{\mathcal{A}} d^2\boldsymbol{\rho}\ (H'(\boldsymbol{\rho}) \ - \ H(\boldsymbol{\rho}))^2 \Big)^{1/2} \tag{6}$$

of H', the helioseismic signature prescribed by $\mathcal{W}$ applied to $\mathcal{H}$, and H itself. We will call Q "the *pole-pairing quality assessor*" for a given $(\mathcal{W},\ \mathcal{H})$, understanding that the highest possible quality is indicated by a deviation that is nil, i.e., an exact fit.

For a beginning development of the practical pole-pairing algorithm, we begin by considering one that identifies, within some domain, the Hale mapping $\mathcal{W}$ that simply minimizes $Q(\mathcal{W},\ \mathcal{H})$ for a given signature, $\mathcal{H}$. It is fairly easy—devising configurations that enjoy certain geometrical symmetries—to contrive pole-pairing problems in which there are two or more Hale mappings with significantly different connectivities for which Q qualifies as both optimal and equal. This introduces an inkling that the practical goal

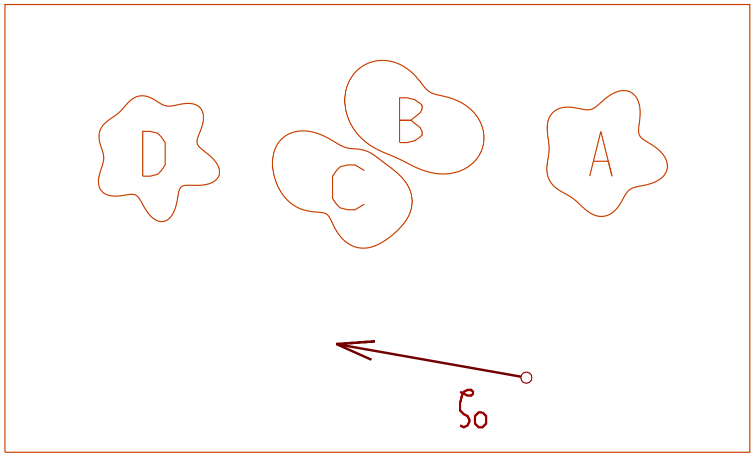

Figure 4. Diagram expressing the components, "A", "B", "C", and "D", of the helioseismic signature of a pair of magnetic bipoles, A–B and C–D, in each of which the separation between the magnetic-north and -south pole is $\boldsymbol{\zeta}_0$.

may could afford to be one of finding one or more mappings, $(\mathcal{W},\ \mathcal{H})$, that are simply "acceptable" based upon some set of criteria, and leaving it to other criteria, yet to be determined, to choose among them if such a choice is desired.

4.3. Distortionless Hale mapping

To illustrate graphically an intuitive approach to the fashioning of a Hale mapping that plausibly addresses the pole-pairing problem, we first note the existence of a class of magnetic regions for which an attractive match can be accomplished by a mapping $\mathcal{W}_0$ that simply translates its argument uniformly by some constant displacement, $\boldsymbol{\zeta}_0$, over $\mathcal{N}$,

$$W_0(\boldsymbol{\rho}) \;=\; \boldsymbol{\zeta}_0, \tag{7}$$

whatever $\mathcal{N}$ is. We will call $\mathcal{W}_0$ a "distortionless mapping", of $\mathcal{N}$ to $\mathcal{S}$, meaning that while it is a substantial non-identity operation involving considerable translation, it happens to involve otherwise *no actual warpage* of $\mathcal{S}$ to conform it to $\mathcal{N}$. Figure 4 shows a conceptual diagram of the helioseismic signature of a magnetic region amenable to modeling in terms of $\mathcal{W}_0$. The active region is composed of two magnetic bipoles, A-B and C-D. Each of these are separated from each other by something close to the displacement represented by the single arrow, representing the vector $\boldsymbol{\zeta}_0$ to be considered for $\mathcal{W}_0$. The task to be undertaken, then, in recognizing and appropriately matching features of leading polarity with their following-polarity counterparts can be regarded as that of an "executor", $\mathcal{E}$, whose function is to examine the helioseismic signature, $\mathcal{H}$, and search the parameter space of $\mathcal{W}$, within the realistic specifications of the Hale

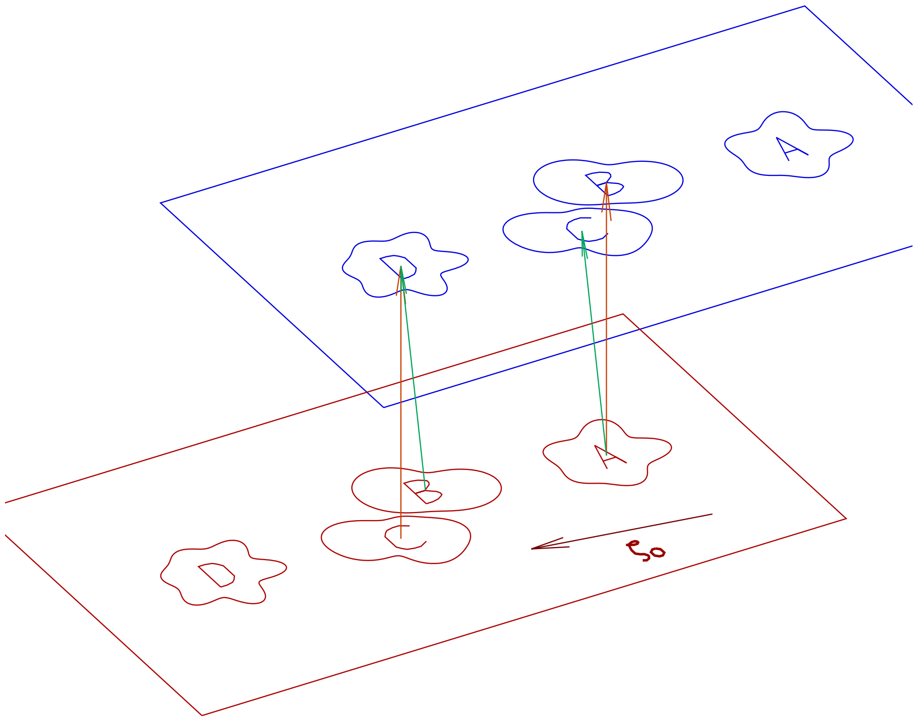

Figure 5. A convenient scheme for assessing relative prospectivities of a magnetic connection between different components of a helioseismic signature consistent with the Hale Polarity Law is attempted by superposing the helioseismic signature shown in Figure 4 (bottom rectangle here) with a version of the same (top rectangle) that is displaced by the nominal Hale displacement vector, $\boldsymbol{\zeta}_0$, but is otherwise unwarped. Positive matches for this $\boldsymbol{\zeta}_0$ are represented by vertical arrows, i.e., accurate superpositions of lobe B and D in the displaced overlay onto A and C, respectively, in the underlying original. It can happen that an alternative choice of $\boldsymbol{\zeta}_0$ will prescribe a similarly positive superposition. In this figure, such an alternative is shown by tilted green arrows, matching C to A and D to B.

Law, for the parameter set (or sets) that minimize Q as prescribed by equation (6).

Figure 5 shows what we might regard to be the executor's vantage into the helioseismic signature, $\mathcal{H}$, diagramed in Figure 4, by overlaying the Hale image (blue rectangle, top) of the helioseismic signature, $\mathcal{H}$, unwarped over the entirety of $\mathcal{A}$ (see equation [2]), on top of the original in $\mathcal{A}$ itself (red rectangle, bottom). The executor should recognize lobes A and C in the original $\mathcal{A}$ (lower, red rectangle), being cospatial with lobes B and D, respectively, in the Hale image, $W(\mathcal{A})$ of $\mathcal{A}$ (upper, blue rectangle) with little deviation for the choice of relative translation, $\boldsymbol{\zeta}_0$, shown. The seismic signatures from which the arrows emanate identify regions to be assigned a leading (magnetic-north) polarity; the arrow heads tag regions to be identified as the respective (magnetic-south) conjugates, The executor should also recognize features A in $W(\mathcal{A})$ (upper, blue) and D in the original (lower, red) that have no cospatial matches. This reinforces A as *not* belonging to $\mathcal{S}$ and D as not belonging to $\mathcal{N}$. The parameter space available to the executor to look for alternative matchings is simply that of the 2-D vector, $\boldsymbol{\zeta}_0$, within confines the executor considers acceptable adherence to the Hale Law.

Where the executor's job begins to get interesting is when, even in the case of a perfectly acceptable match, such as A to B, she finds acceptable alternatives, e.g., A to C (and, accordingly B to D) by an alternative choice of $\boldsymbol{\zeta}_0$. This alternative is represented in Figure 5 by the not-quite-vertical, green arrows connecting lobe A to C, instead of B, and B to D instead of C to D. How to choose between these two possibilities depends upon (1) for which $\boldsymbol{\zeta}_0$ the quality assessment, $Q(\mathcal{W}_0,\ \mathcal{H})$, is lesser, and (2) which $\boldsymbol{\zeta}_0$ the is more in accordance with the executor's understanding of the Hale Law. The inclusion of the condition (2) should be seen as crucial when it is recognized that the least Q is accomplished by the distortionless Hale mapping in which $\boldsymbol{\zeta}_0$ is simply null, which we regard to be securely inconsistent with the Hale Law.

The executor's job becomes still more interesting when there exists a feature, say E, in $\mathcal{N}$, neither the original nor the Hale image (in $\mathcal{S}$) of which is clothed by a cospatial match in the opposing field. The executor is then confronted with two options: (1) admit a more flexible warpage, $\mathcal{W}$, capable of moving E to the location of some matching prospect, or, eventually, (2) recognize the lack of an acceptable match for that feature. We understand that the acceptance of option (2) leaves E naked, hence its polarity ambiguous. This might, for example, be considered as a possible instance in which the magnetic flux that elicits the seismic signature has become connected to interplanetary space, hence having no further connection to the photosphere in the neighborhood of $\mathcal{A}$. This would make E a candidate for a possible coronal hole, and the executor may then see no need for a basis for assigning it to either $\mathcal{N}$ or $\mathcal{S}$ within A.

5. Distortionless Hale mapping applied to a single bipole

AR11416, the subject of Figure 3 is a good example of a region most of whose magnetic flux can be accommodated by a distortionless Hale mapping with an unambiguous displacement, $\boldsymbol{\zeta}_0$. The exercise to follow is facilitated by the development of some specialized tools. These are useful both as components of an algorithm that can play an operational role in space-weather forecasting and for studying the relationship between emerging magnetic regions and their helioseismic signatures, including the evolution of both. We will first illustrate these tools by applying them to NOAA AR11416, which emerged in the southern solar hemisphere in early February of 2012 and is the subject of Figure 3.

5.1. Representation of individual north- and south-magnetic flux densities

Typical magnetic fields on the Sun's surface are known to be stochastic to the extent that there can exist local polarities of opposite sign within the smallest regions resolvable by helioseismic observations. Even in their simplest interpretations, helioseismic signatures (e.g., Fig 3*d*) appear to indicate something like a mean, $\langle \mathcal{H}(\mathbf{B}) \rangle$, of some function, $\mathcal{H}$, of the magnetic field, $\mathbf{B}$, over the region resolved. Helioseismic signatures respond clearly to concentrated magnetic flux, $\langle B_z \rangle$, passing through regions they resolve. An example is availed by comparing frame *b* of Figure 2 with frame *d* of the same. They also remain strong in sharp neutral lines separating regions of strong opposing polarity, i.e., even where $\langle B_z \rangle$, as resolved by magnetograms, passes through zero. An example of this is secured by making the same comparison, frames *b* and *f* in Figure 7. This suggests that the mean magnetic pressure, $\langle B^2/(8\pi) \rangle$, in sharp neutral lines is significantly positive and a major contributor to the helioseismic signature.

The opposing drifts (and to some extent the diffusion) of north- and south-magnetic poles in a given hemisphere are seen to be dependent upon the signs of the respective polarities [6]. This suggests that a useful formalism for a general tool to study the evolution of emerging magnetic flux and its relationship with helioseismic signatures is one that discriminates the distributions of standard north- and south-magnetic polarities by respective non-negative fields, P_n and P_s, recognizing respective north- and south-polar flux densities. These, then respectively denote north- and south-magnetic pole densities, such that

$$\langle B_z \rangle(\boldsymbol{\rho},\ t) \ = \ P_n(\boldsymbol{\rho},\ t) \ - \ P_s(\boldsymbol{\rho},\ t). \tag{8}$$

The appropriation of two fields, P_n and P_s, to express something formerly expressed by only single field, $\langle B_z \rangle$, lends us the facility to express more than B_z alone with the combination of P_n and P_s. For example, we have the flexibility to prescribe that the sum of P_n^2 and P_s^2 represent the mean square magnetic induction, i.e., the "magnetic pressure" except for the factor of 8π:

$$\langle B^2 \rangle(\boldsymbol{\rho},\ t) \ = \ P_n^2(\boldsymbol{\rho},\ t) \ + \ P_s^2(\boldsymbol{\rho},\ t), \tag{9}$$

anticipating that this can serve as a proxy of the helioseismic signature even where the flux density, $\langle B_z \rangle$, is null—whether because $\mathbf{B}$ in a given region contains magnetic flux of both northern and southern polarities within itself, or, possibly, because it can have a horizontal component that can elicit a strong helioseismic signature even where B_z is null.¶

¶ We understand this to be a result of the compressional modulus a horizontal magnetic field presents to upwardly propagating compression waves incident upon it from the solar interior (see discussion of the "penumbral acoustic anomaly" in sunspot penumbrae in Lindsey, Cally and Rempel [10]).

5.2. Relation of individual flux densities to helioseismic signatures

For the actual relationship between $\langle B^2 \rangle$ and the helioseismic signature, H, we adopt the empirical prescription of González et al. [8], who express H as a monotonic function,$^+$

$$H \ = \ \mathcal{J}(\langle B^2 \rangle), \tag{11}$$

of $\langle B^2 \rangle$ as resolved by the seismic monitor. To express $\langle B^2 \rangle$ in terms of H, we invoke the inverse, $\mathcal{B}^2$,* of $\mathcal{J}$, in terms of which

$$\langle B^2 \rangle \ = \ \mathcal{B}^2(H). \tag{13}$$

From equations (9) and (13), then,

$$P_n^2(\boldsymbol{\rho},\ t) \ + \ P_s^2(\boldsymbol{\rho},\ t) \ = \ \mathcal{B}^2(H(\boldsymbol{\rho},\ t)). \tag{14}$$

5.3. Application of distortionless Hale mapping to individual flux densities

In a distortionless Hale mapping, the understanding is that at some moment, t_0, at which we have recognized an element of newly emerged magnetic flux in a helioseismic signature and first take on the problem of discriminating its polarities, the north-magnetic polarities are uniform translations of the south-magnetic polarities,

$$P_s(\boldsymbol{\rho},\ t_0) \ = \ P_n(\boldsymbol{\rho} \ - \ \boldsymbol{\zeta}_0,\ t_0), \tag{15}$$

hence,

$$P_n^2(\boldsymbol{\rho},\ t) \ + \ P_n^2(\boldsymbol{\rho} \ - \ \boldsymbol{\zeta}_0,\ t) \ = \ \mathcal{B}^2(H). \tag{16}$$

When H, hence likewise $\mathcal{B}^2(H)$, is known over a bounded region outside of which it is assured to be nil, equation (16) generally has a standard "practical solution" for $P_n^2(\boldsymbol{\rho})$ in terms of $\mathcal{B}^2(H)$.♯ We express this here in terms of an operator $\mathcal{P}^2(\boldsymbol{\zeta}_0)$ applied to the

$^+$ Formally, for helioseismic signatures in the near hemisphere computed by the prescription that gave us that shown by Figure 3*d*, the helioseismic signature is a travel-time perturbation, $\mathcal{J}$, found to be related to $\langle B^2 \rangle$ by

$$\mathcal{J}(\langle B^2 \rangle) \ \equiv \ h_0 \ln\Big(1 \ + \ \frac{\langle B^2 \rangle}{B_0^2}\Big), \tag{10}$$

with $h_0 \ = \ -15.0$ sec, and $B_0 \ = \ 75$ Gauss.
* $\mathcal{J}$, defined by equation (10), in the previous footnote, is monotonic, and readily inverts to likewise monotonic

$$\mathcal{B}^2(H) \ \equiv \ B_0^2\big(\exp(H/h_0) - 1\big). \tag{12}$$

♯ In general, if $\boldsymbol{\zeta}_0$ has any error, there is any warpage in the real helioseismic signature, or the helioseismic signature has any noise, then equation (16) is cheated out of an exact solution. The "practical solutions" delivered by $\mathcal{B}^2$ applied to H are fits of P_n^2 that attempt to minimize the mean square difference between the left and right sides of equation (16) over $\mathcal{A}$ under appropriate constraints rather than achieve exact equality where none is possible.

field $\mathcal{B}^2(H(\boldsymbol{\rho},\ t_0))$ thus:††

$$P_n^2(\boldsymbol{\rho},\ t_0)\ =\ \mathcal{P}^2(\boldsymbol{\zeta}_0)\mathcal{B}^2(H(\boldsymbol{\rho},\ t_0)). \tag{17}$$

Hence,

$$P_n(\boldsymbol{\rho},\ t_0)\ =\ \Big(\mathcal{P}^2(\boldsymbol{\zeta}_0)\mathcal{B}^2(H(\boldsymbol{\rho},\ t_0))\Big)^{1/2}. \tag{18}$$

An image of P_n prescribed by equation (18) for NOAA AR11416 is shown in Fig 6*c*. The field $P_s(\boldsymbol{\rho},\ t_0)$ now follows by applying equation (15) to $P_n(\boldsymbol{\rho},\ t_0)$. The difference between P_n and P_s, representing B_z, is imaged in Fig 6*e* alongside a line-of-sight magnetogram (Fig 6*f*) for comparison. A control reconstruction of the helioseismic signature [$H'(\boldsymbol{\rho})$ in equation (6)], secured by applying $\mathcal{J}$ to $P_n^2 + P_s^2$, is imaged in Fig 6d, to be compared with the actual helioseismic signature [$H(\boldsymbol{\rho})$ in equation (6)] in Fig 6*b*, directly above.

5.4. Subsequent evolution of newly emerged magnetic flux

Once a fully emerged element of magnetic flux has become apparent on the Sun's surface, it tends broadly to evolve from thence primarily by the opposing polarities drifting apart in roughly opposite directions, generally reinforcing the Hale Polarity Law, in addition to advection by differential solar rotation and meridional flow, also subject to generally anisotropic diffusion [6]. We propose to express this evolution statistically by the application of operators, $\mathcal{E}_n$ and $\mathcal{E}_s$, acting on the respective fields P_n and P_s:

$$\frac{\partial}{\partial t}P_g(\boldsymbol{\rho},\ t)\ =\ \mathcal{E}_g(\theta)P_g(\boldsymbol{\rho},\ t),\ g\ \in\ \{\text{“}n\text{”}, \text{“}s\text{”}\}, \tag{19}$$

where θ represents the local latitude of $\boldsymbol{\rho}$. (I.e., the parameters that quantify the diffusion, drift, advection, etc., depend significantly on solar latitude but are statistically invariant with respect to longitude to our present knowledge.) Temporal invariance of $\mathcal{E}_g$ lets us define of an *evolution operator*,

$$_g(\tau)\ =\ e^{\mathcal{E}_g\tau}, \tag{20}$$

such that

$$P_g(\boldsymbol{\rho},\ t_2)\ =\ U_g(t_2\ -\ t_1)P_g(\boldsymbol{\rho},\ t_1),\ g\ \in\ \{\text{“}n\text{”}, \text{“}s\text{”}\}. \tag{21}$$

Fig 6*g* shows the result of $U_n(\Delta t)$ applied to P_n and $U_s(\Delta t)$ to P_s on 2012-02-12 as represented in panel *d* with Δt a full solar rotation. This is to be compared with a line-of-sight magnetogram of the region at that time, in panel *h*, to its right. The operators $U_n(\Delta t)$ and $U_s(\Delta t)$ make no attempt to reproduce the fine structure of the magnetic flux shown in Fig 6*h*.

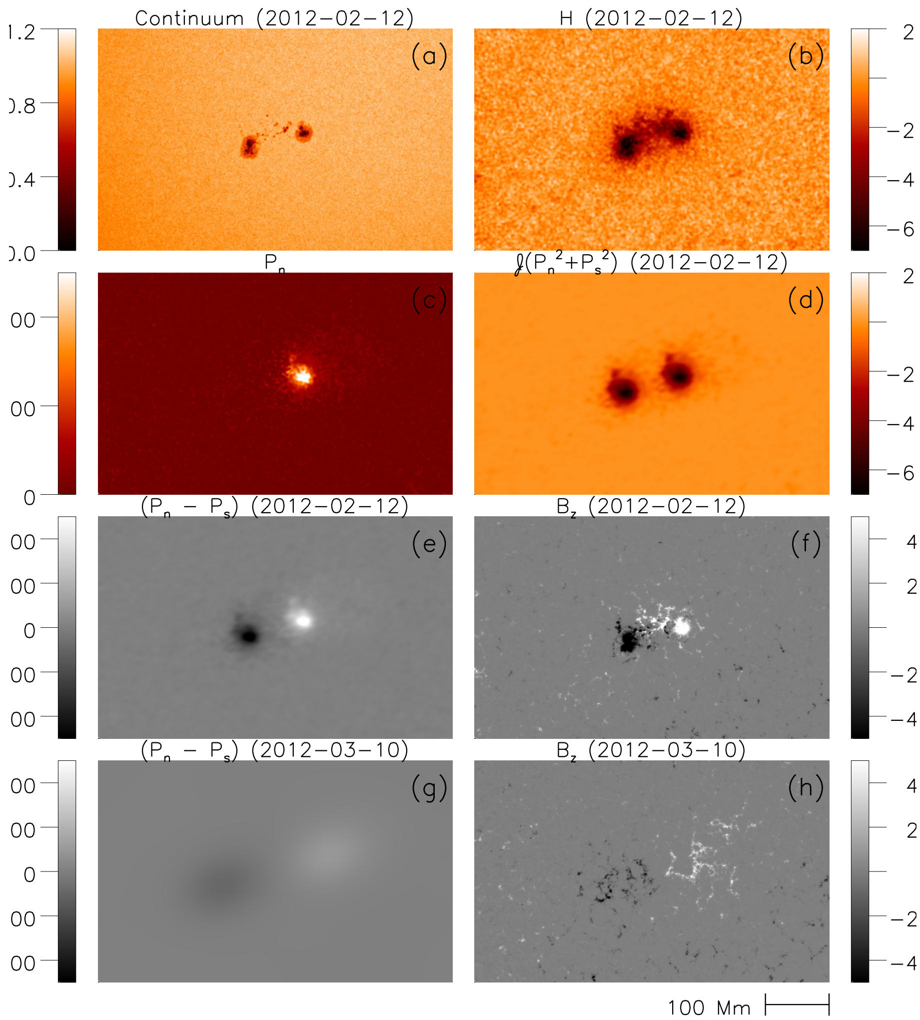

Figure 6. The relationship between helioseimic signatures and the magnetic configurations that give rise to them is illustrated by application of basic analytical tools desribed in the text to observations of NOAA AR11416 as it crosses central solar meridian on 2012-02-12, and again in the succeeding solar rotation. Panel *a* shows the region in the visible continuum on 2012-02-12. Panel *b* shows the concurrent, cospatial helioseismic signature, H, an acoustic travel-time perturbation in units of sec. Panel *c* shows P_n(Gauss), derived from equation (18) applied to the helioseismic signature. Panel *d* shows a control reconstruction of the helioseimic signature derived by applying $\mathcal{J}$ (equation [10]) to $P_n^2 + P_s^2$, where P_s has been derived by equation (15) applied to P_n. Panel *e* shows the magnetic flux density (Gauss) derived by subtracting P_s from P_n, as prescribed by equation (8). Panel *f* shows a concurrent, cospatial line-of-sight magnetogram of the region for comparison. Panel *g* shows the magnetic flux density (Gauss) projected a full solar rotation subsequent to that shown in panel *e* by applying the evolution operators U_n and U_n to P_n and P_n, respectively, for the 27-day synodic solar-rotation period. Panel *h* shows a cospatial line-of-sight HMI magnetogram at that moment.

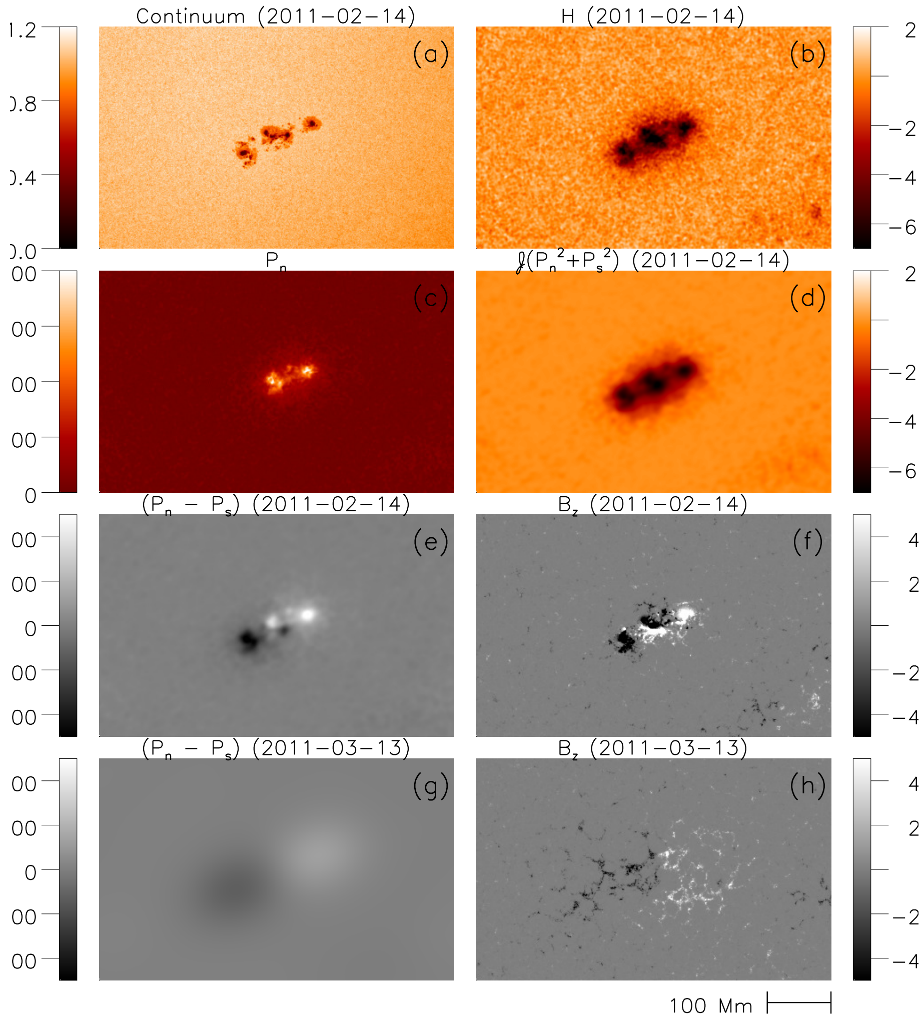

Figure 7. The magnetic extrapolation illustrated in Figure 6 for the simple bipole configuration of NOAA AR11416 is applied here to more magnetically complex NOAA AR11158 (2011-02-13), a region consisting of two bipoles in which the helioseismic signature of the leading pole of the leftward bipole is pressed against the following pole of the more rightward bipole. See caption of Figure 6 for details.

6. Distortionless Hale mapping applied to multiple bipoles

This subject of this § is how distortionless Hale mapping can be extended to active regions consisting of more than a single bipole. The object now is AR11158 circa 2011-02-13, a double bipole that has significant parallels with the idealized active region that was the subject of Figure 4 and 5.

†† Both "$\mathcal{B}^2$" and $\mathcal{P}^2(\boldsymbol{\zeta}_0)$ are intended to indicate the application of a single operation to their respective operands, the superscript indicating simply that the resultant quantities are squares of something. While actually possible, it would be extremely awkward to regard either $\mathcal{B}^2$ or $\mathcal{P}^2(\boldsymbol{\zeta}_0)$ in terms of two successive applications of some operator designated, respectively, "$\mathcal{B}$" or "$\mathcal{P}(\boldsymbol{\zeta}_0)$".

6.1. Best-fit Hale Mapping

Figure 7 shows results of the analysis described in Figure 6 applied to AR11158, minimizing $Q(\mathcal{W},\ \mathcal{H})$ over the full domain of $\boldsymbol{\rho}_0$ outside of the neighborhood of $\boldsymbol{\rho}_0\ =\ 0$. In this case, the leading (up-rightward) north-magnetic pole of the lagging (left-downward) bipole was pressed against the following (left-downward) pole of the leading (up-rightward) bipole, the composite forming the contiguous central lobe of the helioseismic signature (Fig 7*b*). The magnetic-flux distribution prescribed by a distortionless Hale mapping that simply minimizes $Q(\mathcal{W},\ \mathcal{H})$ (Fig 7*e*) is that specified by a leftward $\boldsymbol{\zeta}_0$ whose length is 23 Mm and whose direction is leftward with an inclination pointing 30° downward from the locus of constant latitude. This prescribes a central lobe whose magnetic flux density is artificially weak, due to overlapping of north and south poles that are less relatively displaced from each other than the reality shown in Fig 7*f*. Somewhat worse, the direction of the relative displacement between the north- and south-magnetic components of the central lobe happens to be fundamentally wrong, more than 90° from the reality, i.e., to the left and slightly upward instead of nearly downward. The quality assessor, $Q(\mathcal{W},\ \mathcal{H})$, by itself at least, does not have the leverage to realistically position these components relative to one another within the central lobe. However, the individual values of P_n and P_s opposing each other in the central lobe reserve a collectivity of magnetic flux of both polarities that is quite substantial, thus maintaining a helioseismic signature whose central lobe is appropriately strong (Fig 7*d*). And, the substantiality of P_n and P_s in the central lobe will become apparent in the assessment of B_z as drift in opposing directions pulls the north- and south-magnetic distributions away from one other.

6.2. Hale-compatible quality assessments

There are instances in the physical sciences in which the quality of a fit lends insightful clues about the physics involved. The Hale mapping exercise undertaken in the previous section provides an instance in which, at least at first glance, this need not necessarily be entirely the case. However, when we examine the range of values of $Q(\mathcal{W},\ \mathcal{H})$ over all of $\boldsymbol{\zeta}_0$-space for the helioseismic signature mapped in Fig (7*b*), we find a secondary local minimum in Q at which the length of $\boldsymbol{\zeta}_0$ is 26 Mm with an inclination of just 17°. Figure 8 shows a comparison of the magnetic flux-density map prescribed by this $\boldsymbol{\zeta}_0$, here in frame *d*, and that shown in Figure 7, reproduced here in frame *c*. The magnetic orientation of the central lobe shown here is considerably closer to the reality shown in frame *b* than the one that of the Hale mapping that best fits the helioseismic signature.

While the authors propose in this study rather simply to introduce the question than to resolve it, the proposition is that the shallower inclination is the more statistically compatible with the Hale Law. There is a strong argument, then, for incorporating into the quality assessment introduced by equation (6) an additional component that, while continuing to appeciate the accurate fitting of the helioseismic signature that minimzes

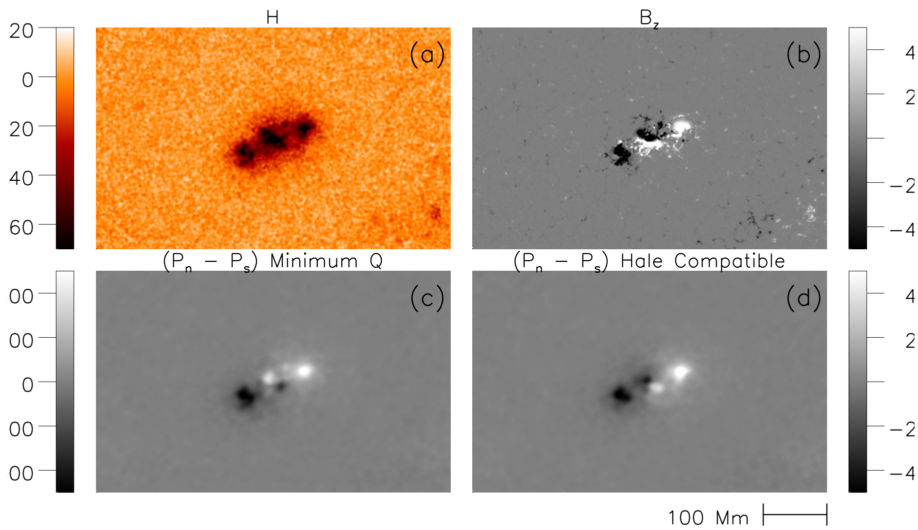

Figure 8. Comparison between magnetic flux density maps prescribed by a distortionless Hale mapping with $\boldsymbol{\rho}_0$ inclined at 30° (frame c), as in Fig 7, which optimizes $Q(\mathcal{W},\ \mathcal{H})$ over the full non-zero $\boldsymbol{\rho}_0$-domain, and the same for $\boldsymbol{\rho}_0$ inclined at 17° (frame d), which admits a greater deviation of $Q(\mathcal{W},\ \mathcal{H})$ from a perfect fit, but which we propose is more compatible with the Hale law.

$Q(\mathcal{W},\ \mathcal{H})$, appropriately discourages the attainment of this by excessive departures from a nominal domain known to be the most statistically compatible with the Hale Law. The case illustrated in Figure 8 might could be regarded as a single datum in the statistics needed to develop such a component.

7. Avenues for further development of the problem: Hale mappings that can accommodate distortion

The tools we have demonstrated in this study have straight-forward extensions to Hale mappings capable of expressing real distortion in magnetic connectivities from $\mathcal{N}$ to $\mathcal{S}$. This entails mapping functions, $W(\boldsymbol{\rho})$, that are now capable of some degree of variation dependent upon their argument, $\boldsymbol{\rho}$. The existence of active regions in which distortionless Hale mapping works moderately well suggests the existence of a more substantial class of active regions for which W could be expressed alytically in some sense. To wit,

$$W(\boldsymbol{\rho}) \ = \ \boldsymbol{\zeta}_0 \ + \ W_1(\boldsymbol{\sigma};\ \boldsymbol{\rho}_1), \tag{22}$$

where $\boldsymbol{\rho}_1$ is the deviation of $\boldsymbol{\rho}$ from some reference point $\boldsymbol{\rho}_0$ in $\mathcal{N}$ which W maps to $\boldsymbol{\zeta}_0$, $\boldsymbol{\sigma}$ represents a set of warping parameters, and $W_1(\boldsymbol{\sigma};\ \boldsymbol{\zeta}_1)$ is an "analytic" function of $\boldsymbol{\rho}_1$ that is null at 0—keeping in mind that the manifold of $\boldsymbol{\rho}_1$ is 2-dimensional.

Analytic distortions would be fully capable of mapping two separate regions in $\mathcal{N}$ into the same location in $\mathcal{S}$, forming the optical analog of caustics and stigmas therein. These are perhaps more appropriately accidents to be avoided than welcome flexibilities. The ability to devise such singularities accidentally might complicate simpler methods, such as linear regression, of searching the parameter space of $\mathcal{W}$, for realistic connectivities. By the same token, though, analytic distortions also have the flexiblity and power to accommodate non-trivial magnetic topology, such as in pairs of bipoles one of whose coronal magnetic streamlines cross over or under those of the other. This is a highly appropriate facility for realistic Hale mapping to offer. EUV observations of magnetic loops of active regions consisting of multiple bipoles, then, offers a very attractive resource for the exploration of analytic Hale mapping in which distortion is important.

8. Summary

Since the turn of the century, we have been using seismic observations of the Sun's near hemisphere to monitor large active regions in the far hemisphere for applications in space-weather forecasting. Helioseismic signatures give us realistic morphologies of magnetic flux densities, but not their signs, i.e., whether a given lobe of the signature is predominately of north- or south-magnetic polarity. N. Arge and C. Henney [7] introduced the idea of using the Hale Polarity Law to assign appropriate magnetic polarities to active regions that can be accurately represented as single magnetic bipoles. This is based upon a strong tendency for emerging active regions to consist of bipolar components with consistent leading and following polarities in either hemisphere during a given solar cycle.

This study addresses the more general problem of assigning appropriate polarities to more complex magnetic configurations, active regions consisting of multiple magnetic bipoles. Following the lead of MacDonald et al. [9], this study is conducted in the Sun's near hemisphere, where helioseismic signatures can be compared with concurrent line-of-sight magnetic observations. The heart of our approach is an algorithm that formulates a "Hale mapping" of the helioseismic signature of the subject. The Hale mapping partitions the helioseismic signature into distinctive regions of north- and south-magnetic polarity and proposes magnetic connectivities between respective north and south components. The algorithm is based upon identifying the Hale-mapping parameters that optimally fit the helioseismic signature under appropriate constraints.

We have successfully applied the algorithm to active regions that can be accurately fit to what we call distortionless Hale mappings, i.e., regions in which the separations between opposing polarities are uniform over the helioseismic signature—even where there can be overlap of regions containing north- and south-polar magnetic flux. The goal is to extended the applicability to magnetic regions in which these separations, both their magnitude and direction, can vary with location.

Acknowledgments

Nick Arge and Carl Henney introduced the application of the Hale Polarity Law to

STEREO EUV images of active regions in the Sun's far hemisphere to model active regions there as single bipoles. They extended this method to helioseismic images of active regions in the far hemisphere, and use the results to improve models of the global coronal magnetic field. We appreciate their insight—and foresight—very much. We appreciate closely related work by Gordon MacDonald comparing helioseismic signatures with magnetic maps in the Sun's near hemisphere. We greatly appreciate Dr. Joseph Werne's review of this study, and Janet Biggs's editorial review of the manuscript. This work was supported by contracts with the National Oceanic and Atmospheric Administration's (NOAA's) Small Business Inovative Research (SBIR) program and the National Aeronautics and Space Administration's (NASA's) SunEarth Connection GuestInvestigator Program.

References

[1] Lindsey, C and Braun, D C 1990 *Solar Phys.* **126**, 101
[2] Lindsey, C and Braun, D C 1997 *ApJ* **485**, 895
[3] Donea A-C, Braun D C and Lindsey C 1997 *ApJL* **513**, 143
[4] Lindsey, C and Braun, D C 2000 *Science* **287**, 1799
[5] Braun, D C and Lindsey, C 2001 *ApJL* **560**, 189
[6] Wang Y-M, Nash A G and Sheeley N R Jr 1989 *Science* **245**, 712
[7] Arge, N C, Henney, C J, González Hernández, I and Toussaint, W A 2013 *AIPC* **1539**, 11
[8] González Hernández, I, Hill, F and Lindsey, C 2007 *ApJ* **669**, 1382
[9] MacDonald G A, Henney C J, Díaz Alfaro M, González Hernández I, Arge, C N, Lindsey, C and McAteer R T J 2015 *ApJ* **807**, 21
[10] Lindsey, C, Cally, P S and Rempel, M. 2010 *ApJ* **719**, 1144
[11] Herstein, I. N. 1964 *Topics in Algebra* (Wiley, New York) p. 10